Special issue article

X-RAY SPECTROMETRY

Published online in Wiley Online Library: 3 July 2015

(wileyonlinelibrary.com) DOI 10.1002/xrs.2634

Prospects of X-ray photoemission electron microscopy at the first beamline of the Polish synchrotron facility 'Solaris'

M. Ślęzak,[a,b]* T. Giela,[c] D. Wilgocka-Ślęzak,[c] N. Spiridis,[c] T. Ślęzak,[b] M. Zając,[d] A. Kozioł-Rachwał,[b] R. P. Socha,[c] M. Stankiewicz,[d] P. Warnicke,[a] N. Pilet,[a] J. Raabe,[a] C. Quitmann[a] and J. Korecki[b,c]

The synchrotron radiation facility 'Solaris' is currently being built in Krakow, Poland. The first experimental beamline at Solaris will use bending magnet radiation and two exchangeable end stations: a spectroscopic X-ray photoemission electron microscope and a soft X-ray absorption spectroscopy chamber. We present the beamline specifications and exemplary results obtained with our end station microscope, which (*in statu nascendi* of Solaris) has been operated at the NanoXAS beamline in the Swiss Light Source. The end stations should be available for a broad user community at Solaris in 2016. Copyright © 2015 John Wiley & Sons, Ltd.

Introduction

X-ray photoemission electron microscopy (XPEEM) has recently become a frequently used and powerful spectro-microscopic technique for the investigation of nanostructures, surfaces, interfaces, thin films and buried layers.[1,2] Its intensive use is mainly because of the increasing availability of third generation synchrotron facilities as well as progress in electron optics design. In this paper, we present a concept for a soft X-ray microscopy and spectroscopy beamline, which will be the first experimental line at Solaris, the synchrotron facility currently under construction in Krakow, Poland.[3] The beamline layout and its primary end station, i.e. the Elmitec spectroscopic PEEM III microscope, are described. In the framework of Swiss–Polish cooperation, the microscope has been installed and operated for several weeks at the NanoXAS beamline[4] at the Swiss Light Source (SLS). The capabilities of the XPEEM chemical and magnetic spectro-microscopy and micro-spectroscopy are demonstrated using results obtained during a series of experiments at SLS.

Soft X-ray micro-spectroscopy beamline at Solaris

The Polish national synchrotron light source 'Solaris', which was approved for construction in February 2010, is based on the small storage ring of the Max IV project in Lund, Sweden.[5] The storage ring will have a 96-m circumference with a 500-mA current and an electron energy of 1.5 GeV.[3] There are four or five experimental beamlines planned in the first phase that will be operated with a dozen end stations. Currently, the building is ready, the machine installation has just finished and approaches commissioning phase. The assembly of the first experimental beamline has begun at the end of 2014, and the beamline is planned to be commissioned in the middle of 2016.

The first beamline will be dedicated to soft X-ray spectroscopy and micro-spectroscopy measurements, which will be achieved with two alternative end stations. The first end station will be a universal chamber for X-ray absorption spectroscopy (XAS), which will also enable X-ray magnetic circular and linear dichroism measurements, similar to the end station E3 at the SIM beamline at SLS.[6] The end station will be devoted to standard spectroscopic measurements in external magnetic and electric fields for various solid and thin film samples over a broad temperature range.

The second end station, the spectroscopic photoemission electron microscope, will be used for surface, thin film and nanostructure studies on conductive samples compatible with ultrahigh vacuum (UHV) conditions. The XPEEM technique offers full field real-time imaging with a lateral resolution down to over a dozen nanometres[7] (routinely several tens). Because of a short mean free path of electrons in solids,[8] the method probes approximately a 5-nm-thick surface layer. By measuring the XAS spectrum and tuning the photon energy to the absorption edge of a particular element in the sample, one can make use of element selective imaging and determine the chemical properties of the sample. In this case, the effective imaging is achieved using highly intense inelastic secondary electrons. Deeper insight into the chemical state of the sample can be obtained when characteristic photoelectrons or Auger electrons rather than secondary electrons are used for imaging and spectroscopy with an instrument equipped with an electron energy analyser.[9]

* *Correspondence to: M. Ślęzak, Swiss Light Source, Paul Scherrer Institut, Switzerland. E-mail: mislezak@agh.edu.pl*

a *Swiss Light Source, Paul Scherrer Institut, Switzerland*

b *Faculty of Physics and Applied Computer Science, AGH, Kraków, Poland*

c *Jerzy Haber Institute of Catalysis and Surface Chemistry PAS, Kraków, Poland*

d *National Synchrotron Radiation Centre SOLARIS, Jagiellonian University, Kraków, Poland*

By taking advantage of the tuneable helicity (circular right, left and linear) of incoming light, the method has routinely been used for imaging magnetic domains in thin films and nanostructures.[10] In this case, high intensity secondary electrons are used, and magnetic contrast is usually obtained using X-ray magnetic circular and linear dichroism effects (XMCD[11] and XMLD[12]) for ferro- and antiferromagnets, respectively.

The beamline will use X-rays from a bending magnet. The beamline layout is illustrated in Fig. 1.

The dispersed beam from the bending magnet is first reflected by a toroidal mirror, which collimates light in the vertical plane and focuses horizontally at the exit slit (ES) position. The collimated light illuminates a plane grating monochromator (PGM), which contains two exchangeable gratings. The grating grooves density was selected to be 800 l/mm and 1600 l/mm to deliver a monochromatic beam in the energy range of 200 eV to 1800 eV with an ultimate resolving power of $E/\Delta E \approx 5000$. This energy range covers the absorption K edges for light elements, from carbon to silicon, L edges of elements with Z between 20 and 40, including 3d elements and also M edges of many heavier atoms, including 4d elements. The energy resolution can be optimised (at the cost of intensity) by closing the ES. The monochromatic beam will be focused vertically on the ES by a cylindrical mirror with a dispersion length of 7.5 m. A toroidal mirror downstream the ES will refocus the photon beam in both directions at the ratio of 1:1.5. The calculated focal spot size (FWHM) at the sample position of the primary end station (PEEM) is $40 \times 100\ \mu m^2$ (v × h). Because of the grazing incidence geometry of the incoming radiation (16° with respect to the sample surface) the beam footprint on the sample increases to 360 μm in the horizontal direction.

Between the ES and the refocusing mirror, a second end station (XAS chamber) can be inserted. Spectroscopic experiments will be available using a millimetre-sized divergent beam.

The selection of the beam polarisation (linear, left or right) will be realised with a mechanical shutter placed after the first collimating mirror. For quantitative measurements (such as XMCD spectroscopy), the integral photon flux will be monitored using a photoemission current diagnostic either before the PEEM end station or before the last optical element (refocusing mirror).

Selected XPEEM applications

The following subsections exemplify possible applications of the XPEEM technique. The presented results were obtained using the Elmitec spectroscopic PEEM III instrument with a hemispherical energy analyser. The microscope intended for 'Solaris' was temporarily installed and tested at the NanoXAS bending magnet beamline at SLS. The instrument is equipped with an UHV preparation chamber including a low energy electron diffractometer and a molecular beam epitaxy (MBE) facility. Deposition sources are also available in the main microscope chamber; thus, direct observation of growth processes is possible.

XPEEM spatial resolution

The best spatial resolution of approximately 15 nm was demonstrated using secondary electron imaging for self-organised Fe stripes prepared on a W(110) single crystal by annealing of a 10 ML (monolayer) thick Fe film at 600 °C.[13] The acquisition time of the image presented in Fig. 2 was 10 s. A fit of the Gauss error function to the section profile presented in Fig. 2 resulted in a spatial resolution of 15 nm.

The resolution can be improved further by reducing chromatic aberrations using monoenergetic photoelectrons,[7] which was in our case limited by the available intensity of the X-ray beam. Nevertheless, considering the intrinsic contribution to the resolution resulting from the spatially extended edges of the several monolayers high Fe-stripe, the achieved resolution compares well with the best data reported for state of the art instruments.[7] Compared with the temporal setup at SLS, the 'Solaris' beamline will benefit from additional refocusing optics. Over one order of intensity gain is thus expected, which should allow more complex XPEEM experiments with reasonable acquisition times.

Selected area X-ray photoemission spectroscopy

X-ray photoemission spectroscopy (XPS) is performed by exciting a sample with fixed energy X-rays and measuring the kinetic energy of the core-level photoelectrons escaping from the irradiated sample. In this manner, one probes the chemical states of the emitting

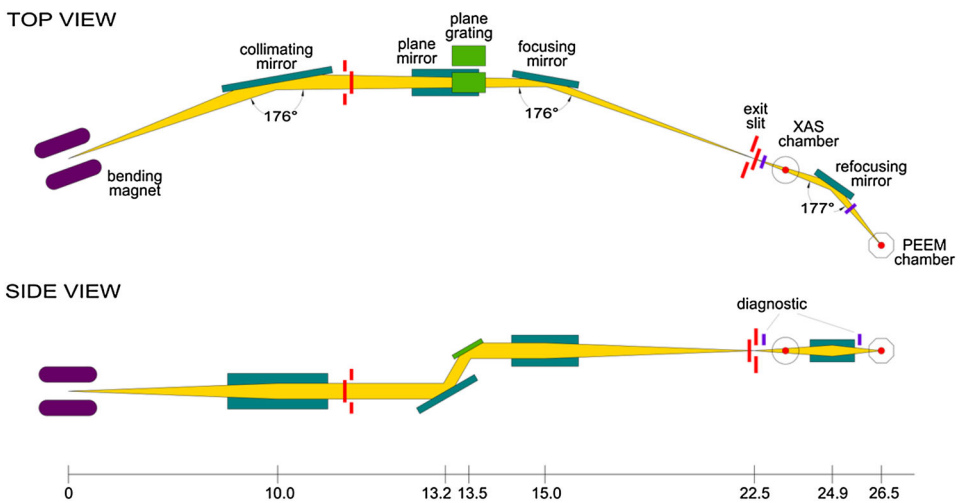

Figure 1. Top and side views of the optical layout of the spectro-microscopy beamline (not to scale) showing the bending magnet source followed by the collimating mirror, plane grating monochromator and focusing mirror. The divergent monochromatic beam can be employed for experiments in a movable XAS end station. An additional refocusing mirror will be used to collimate the beam for XPEEM experiments.

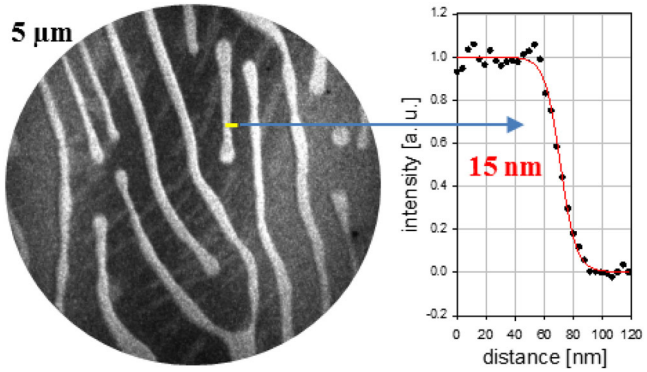

Figure 2. XPEEM images of Fe stripes on a W(110) single crystal at the Fe L3 edge. The field of view (FOV) diameter was 5 µm. The intensity profile across an Fe stripe demonstrates the spatial resolution of 15 nm. The resolution was determined as the width at which the intensity changed from 20% to 80%.

atoms by measuring the electron binding energies. For PEEM, the analysis of the photoelectrons can be additionally restricted to a selected sample area. In Fig. 3(a), a secondary electron XPEEM image of a thin film magnetite sample is presented. This epitaxial 400-Å Fe_3O_4/150-Å Fe/MgO(001) sample was prepared *ex situ* and, after introduction to the microscope, was annealed at 550 °C for 30 min under UHV conditions to restore the surface quality. The XPEEM image, acquired at the Fe L3 edge, revealed two different sample areas, marked as A and B in Fig. 3(a). The corresponding O 1s and Fe $2p_{3/2}$ photoemission spectra are presented in Fig. 3(b) and 3(c), respectively.

The position of the main features of the Fe photoemission spectra indicates that the annealing resulted in local changes to the oxide film stoichiometry. The maximum of Fe $2p_{3/2}$ core excitation for area B was shifted to lower electron binding energies, which is typical for Fe^{2+} (stoichiometry close to FeO); in contrast, for area A, which dominated the surface, the typical features of Fe_3O_4 were observed. With a higher intensity beam, measurements of this type would allow a chemical map of the surface to be constructed.

Selected area XAS and element selective imaging

The XPEEM micro-spectroscopic capabilities can be best exploited for multicomponent or structured samples, such as multilayers and wedge-shaped samples used for thickness dependent studies. An example of such a sample is an epitaxial Fe/Au/Co structure grown on W(110). The base 200-Å Fe(110) layer is followed by a (111)-oriented 7-Å Au film. Using a shutter in front of the tungsten crystal, a part of the sample was covered with 20 Å of cobalt. In this manner, at the border between the Fe/Au bilayer and the exchange coupled Fe/Au/Co trilayer, a Co microwedge was formed with a thickness ranging from 0 to 10 ML, as determined by the quartz microbalance. In Fig. 4(a), an image of the Co microwedge area is presented, which was obtained as a difference between two images: the first one taken at the L3 edge of Co and the second one at the pre-edge energy (i.e. 10 eV below). The intensity changes across the image, from the dark area, without cobalt, to the bright area, where the Co thickness saturates at 10 ML, can be quantitatively examined by analysing the local XAS spectra. The XAS spectra for the Fe/Au and Fe/Au/Co areas are presented in Fig. 4(b) as A and B, respectively.

The intensity profile (Fig. 4(c)) demonstrates that the thickness of the Co layer can be precisely determined at a given position on the sample. This simple example of selected area XAS spectroscopy and element selective imaging with XPEEM can be applied to the study of phase or spin reorientation transitions (SRT).

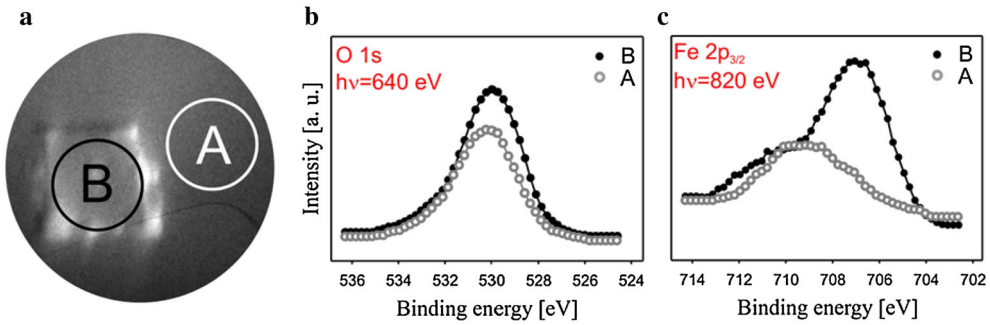

Figure 3. a) Secondary electron XPEEM image of a 400-Å Fe_3O_4/150-Å Fe/MgO(001) sample after 30 min of annealing at 550 °C in UHV. The incoming X-ray energy was 707 eV (Fe L3 edge), and the FOV was 5 µm. (b) O 1s and (c) Fe $2p_{3/2}$ core-level X-ray photoelectron spectra acquired from the areas A (white dots) and B (black dots), as indicated by the white and black circles in (a), respectively. The acquisition time of a single spectrum was 8 min.

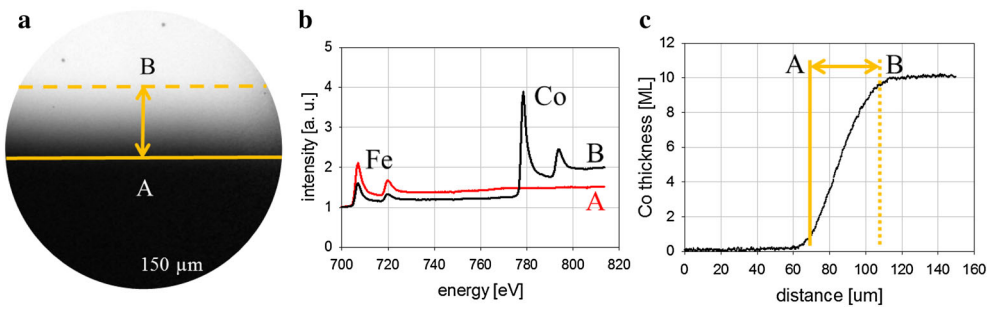

Figure 4. (a) Differential image of Co distribution in a microwedge and the surrounding area of the sandwiched Fe/Au/Co sample described in the text. The FOV was 150 µm. (b) XAS spectra taken at positions A and B. (c) The L3 Co intensity profile across the Co microwedge. The vertical lines refer to the corresponding lines in (a). The Co thickness scale is derived within the linear thickness–intensity relation.

Imaging with magnetic contrast

The circular polarisation of the X-rays at the NanoXAS beamline was changed by moving the sample vertically across the beam. When the sample was in the beam centre, the imaged area was illuminated with linearly polarised X-rays, whereas for the upper and lower beam edges, elliptical polarisations with opposite helicity were available. An imaging example using the magnetic contrast is presented in Fig. 5(a), showing an XMCD image of two antiparallely magnetised domains in a 120-Å epitaxial Fe film on W(110). The presented image is the difference of two images taken at the L3 Fe absorption for opposite helicities of incoming light.

Similar to the local chemical sensitivity presented in the previous section, the magnetic imaging can be accompanied by magnetic micro-spectroscopy, if a series of images as a function of X-ray energy is collected. In this manner, a collection of XAS and XMCD spectra can be obtained, with the ultimate spatial resolution corresponding to the size of a single image pixel. In contrast to integral XMCD spectroscopy, meaningful information can be obtained without a magnetic field for the magnetically unsaturated samples, when the XMCD-asymmetry spectrum is constructed from the XAS spectra derived from different domains, as demonstrated in Fig. 5(b). The XAS spectra (top) acquired with circularly right polarised light from two areas of interest, marked in the image, are combined into the XMCD spectrum (bottom). Using the sum rules from the XMCD spectrum, the spin and orbital magnetic moments can be extracted, provided that the experimental conditions enable proper quantitative analysis.[14] Whereas the absolute values of the magnetic moment can be to some extent ambiguous (because of the uncertainty of the magnetisation direction), this type of XMCD spectroscopy can be very useful in directly comparing the magnetic property variation across inhomogeneous samples. This type of sample can be fabricated either artificially (e.g. wedge samples) or formed by self-organisation, as, for example, Fe stripes on W(110) (compare the image in Fig. 2 obtained with the linearly polarised X-rays). Combined XAS (not shown) and XMCD imaging (Fig. 5(c)) reveals that the ferromagnetic Fe stripes are surrounded by a paramagnetic Fe-monolayer 'sea'. From scanning tunnelling microscopy (not shown), we know that the Fe stripes, which cross many W(110) monoatomic steps, expose their atomically flat (110) surface. There are four types of magnetic contrast visible in the image, corresponding to four types of magnetic domains within the Fe stripes. The long arrows in Fig. 5(c) show an example of two stripes with opposite magnetisations along the stripe axis, i.e. along two opposite <001> directions, as indicated by the black and white contrast. Stripes with the [1$\bar{1}$0]-type easy axis (intermediate grey contrast, short arrows), as well as some multi-domain stripes with all four types of magnetic domains inside are also present. Similar Fe stripes were studied by Zdyb et al.[15] These authors concluded that the shape anisotropy is decisive for the observed spin reorientation transition; however, the coexistence of different easy directions within a single stripe suggests that SRT induced by a thickness gradient may have also occurred.

In addition, more advanced studies, including measurements in small external magnetic and electric fields and local hysteresis loop measurements on the nanometre scale, are possible using XMCD–PEEM, as recently reviewed by Le Guyader et al.[16]

Imaging with combined chemical and magnetic sensitivity

An example of combined element and magnetic specific XPEEM studies in a single experiment is shown in Fig. 6, where the element selectivity is exploited to image the magnetic domain structure in 200-Å Fe/7-Å Au/20-Å Co trilayers grown in situ on W(110) (preparation details in Section on Selected Area XAS and Element Selective Imaging).

Magnetic domain structures were imaged for both magnetic sublayers by tuning the L3 absorption edges of Fe (Fig. 6(a)) and Co (Fig. 6(b)). Inside the domains, the magnetisation direction of Fe is reflected in the Co layer—the Fe and Co layers are ferromagnetically coupled. This coupling can be easily understood in terms of the interlayer exchange interaction dependence on the Au spacer thickness,[17] which, for the 7-Å-thick Au layer, can result in ferromagnetic interaction between the Co and Fe sublayers. However, at the domain borders, a secondary domain structure is observed with antiparallel (AP) Co and Fe magnetisation alignment, as shown schematically by arrows in the Fig. 6. This secondary structure can be better visualised based on the image obtained as a difference between the Fe and Co XMCD images (Fig. 6(c)). It is unlikely that in these AP border regions the interlayer coupling locally changes its sign, and we attribute this surprising effect to magnetostatic coupling because of stray fields originating from the underlying Fe domain walls.[18] A closer examination of the iron image (Fig. 6(a)) reveals small changes of the contrast in the areas corresponding to the AP areas: in the dark domain, the AP areas are slightly brighter, whereas in the bright domain, the AP areas are slightly darker (on the cobalt image, this effect is not observed). This finding implies that the presence of the cobalt domain walls also

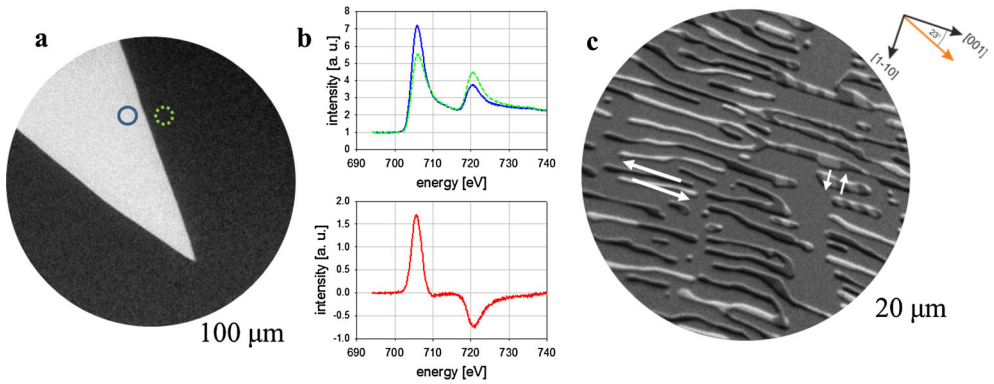

Figure 5. a) XMCD–PEEM image of an epitaxial Fe film on a W(110) single crystal at the Fe L3 edge (FOV 100 µm), and b) the XAS spectra from the areas marked with circles in a) (top) and their difference, i.e. the XMCD spectrum (bottom), are plotted. c) XMCD–PEEM image (FOV 20 µm) of epitaxial Fe nanostripes on W(110). The incoming radiation wave vector projected on the (110) sample plane made an angle of 23° with the [001] in-plane crystallographic direction.

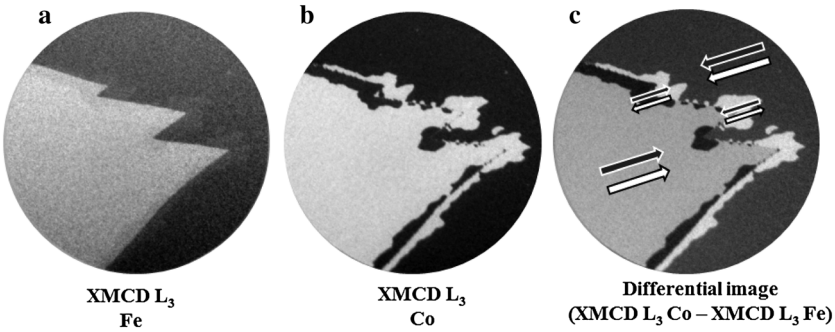

Figure 6. Magnetic domain structures in Fe/Au/Co trilayers grown on W(110) as observed by XMCD–PEEM. The arrows indicate the relative magnetisation alignment of the Fe and Co layers (FOV 37.5 μm).

affects the local magnetic order of iron and slightly deflects its magnetisation from the [001] direction. Therefore, the angle between magnetic moments of the Fe and Co sublayers in the 'AP areas' is slightly different than 180°.

Real-time imaging

The set of images presented in Fig. 7 show the evolution of the magnetic structure during the thickness-induced in-plane spin reorientation transition (SRT) in Fe/W(110).[13] All the XPEEM images presented in this Section are the single frames from a movie recorded during the growth of the Fe film at the Fe L3 edge for the circularly polarised photons.

For the 45-Å-thick Fe film, three types of magnetic domains are present in the sample, namely, the two opposite [001] magnetic domains surrounded by an extended area where the Fe film is homogenously magnetised along $[1\bar{1}0]$. With increasing Fe thickness (Fig. 7(b–d)), the in-plane SRT from $[1\bar{1}0]$ to [001] proceeds by continuous growth of the [001]-magnetised domains.

For details concerning this SRT process, the reader is referred to.[13] From the methodological viewpoint it is important to note that the XPEEM images presented in Fig. 7 are single frames from a movie recorded during the Fe film growth and that the exposure time per frame was only 0.2 s. These results demonstrate the usefulness of the XPEEM technique for studying slowly varying physical processes in real time.

Summary and outlook

We presented the concept of the first experimental beamline at Solaris, the Polish synchrotron currently under construction. Selected results obtained with our PEEM microscope at Swiss Light Source demonstrate the capabilities of this future end station and how chemical and magnetic sensitivity can be combined in spectro-microscopic and micro-spectroscopic measurements. The beamline with its end stations should be available for external users in 2016.

In comparison to the temporary installation at SLS, at the first SOLARIS beamline the performance of the PEEM microscope is expected to be considerably enhanced. This is the consequence of the non-optimum focusing condition at SLS, where PEEM installation was limited by the existing solutions which resulted in a big beam spot on the sample. Within the planned configuration of the beamline optics, for the optimal choice of the grating the expected spectral flux [photons/s/0.1% BW] at the sample is 2×10^{11} and 1×10^{11} in the energy range of 200–1400 eV and drops to 5×10^{10} at 1600 eV and 2×10^{10} at 1800 eV. Taking into account the source flux and the optical layout of the beamlines at SLS and SOLARIS over one order of magnitude of the intensity improvement at SOLARIS can be expected, especially for small fields of view. Moreover the unique solution of the double-bend achromats applied in the SOLARIS storage ring should stop the beam fluctuations[19] and give a low emittance beam. Another important feature is the polarisation switching between different helicities which is essential for the XMCD measurements. At SOLARIS this will be done by selecting appropriate beam part (above or below the electron orbit) with the use of slits placed before the monochromator, without any influence on the energy calibration and resolution at the sample position. From the beamline calculations we find that the circular polarisation of 80% can be achieved with 30% of the total flux. Finally, the online monitoring of the beam intensity available at SOLARIS will allow quantitative analysis of the XAS and XMCD spectra.

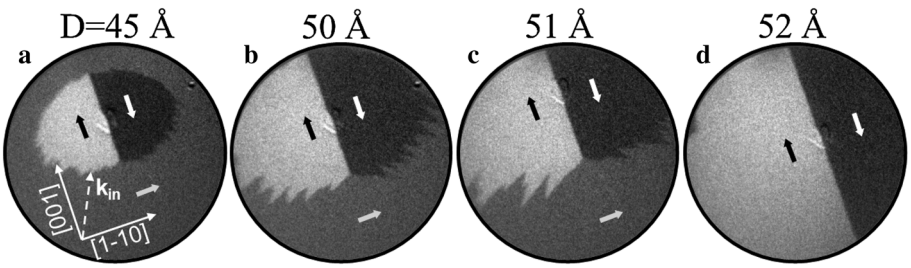

Figure 7. In-plane thickness-induced SRT in Fe/W(110) observed using XPEEM with circularly polarised X-rays at the Fe L3 edge. The in-plane component of the incoming radiation wave vector forms an angle of 23° with the [001] in-plane crystallographic direction. The arrows indicate the magnetisation orientations in each domain. The images are single frames extracted from a movie recorded during the growth of the Fe film. The film thickness *D* is indicated. The position of a defect at the domain border changes because the sample was moved along the [001] direction. The FOV was 150 μm.

Acknowledgements

The SOLARIS and PEEM projects were funded by EU European Regional Development Fund. This work was supported in part by the Scientific Exchange Programme NMS-CH (SCIEX) project, by the National Science Center (NCN), Poland (Grant No. 2012/06/M/ST4/00032), the TEAM Program of the Foundation for Polish Science (co-financed by the EU European Regional Development Fund) and the Marian Smoluchowski Krakow Research Consortium (the Leading National Research Centre, KNOW, which is supported by the Polish Ministry of Science and Higher Education).

Invaluable help of many colleagues from PSI, especially F. Nolting, A. Kleibert and B. Sarafimov, in installation and running of Polish PEEM at SLS is gratefully acknowledged.

References

[1] A. Locatelli, E. Bauer. Recent advances in chemical and magnetic imaging of surfaces and interfaces by XPEEM. *J. Phys. Condens. Matter* **2008**, *20*, 093002.
[2] H. Ohldag, T. J. Regan, J. Stöhr, A. Scholl, F. Nolting, J. Lüning, C. Stamm, S. Anders, R. L. White. Spectroscopic identification and direct imaging of interfacial magnetic spins. *Phys. Rev. Lett.* **2001**, *87*, 247201.
[3] M. R. Bartosik, *et al*. Solaris—National synchrotron radiation centre, project progress, May 2012. *Radiat. Phys. Chem.* **2013**, *93*, 4.
[4] N. Pilet, J. Raabe, S. E. Stevenson, S. Romer, L. Bernard, C. R. McNeill, R. H. Fink, H. J. Hug, C. Quitmann. *Nanotechnology* **2012**, *23*, 475708.
[5] MAX IV Detailed Design Report, www.maxlab.lu.se/node/1136 **2010**.
[6] http://www.psi.ch/sls/sim/endstations#Endstation_ES3_X_ray_Magnetic_Ci
[7] T. Schmidt, A. Sala, H. Marchetto, E. Umbach, H.-J. Freund. First experimental proof for aberration correction in XPEEM: resolution, transmission enhancement, and limitation by space charge effects. *Ultramicroscopy* **2013**, *126*, 23–32.
[8] J. Powell, A. Jablonski. Evaluation of calculated and measured electron inelastic mean free paths near solid surfaces. *J. Phys. Chem. Ref. Data* **1999**, *28*, 19.
[9] T. O. Mentes, A. Locatelli. Angle-resolved X-ray photoemission electron microscopy. *J. Electron Spectros. Relat. Phenom.* **2012**, *185*, 323–329.
[10] W. Kuch. X-ray magnetic circular dichroism for quantitative element-resolved magnetic microscopy. *Phys Scripta* **2004**, *T109*, 89–95.
[11] G. Schütz, W. Wagner, W. Wilhelm, P. Kienle, R. Zeller, R. Frahm, G. Materlik. *Phys. Rev. Lett.* **1987**, *58*, 737.
[12] A. Scholl, H. Ohldag, F. Nolting, S. Anders, J. Stöhr. Study of ferromagnet-antiferromagnet interfaces using X-ray PEEM, in *Magnetic Microscopy of Nanostructures* (Eds: H. Hopster, H. P. Oepen), Springer-Verlag, Berlin Heidelberg, **2005**, pp. 29–48.
[13] M. Ślęzak, T. Giela, D. Wilgocka-Ślęzak, A. Kozioł-Rachwał, T. Ślęzak, R. Zdyb, N. Spiridis, C. Quitmann, J. Raabe, N. Pilet, J. Korecki. X-ray photoemission electron microscopy study of the in-plane spin reorientation transitions in epitaxial Fe films on W(110). *J. Magn. Magn. Mater.* **2013**, *348*, 101–106.
[14] W. Kuch, J. Gilles, F. Offi, S. S. Kang, S. Imada, S. Suga, J. Kirschner. Element-selective mapping of magnetic moments in ultrathin magnetic films using a photoemission microscope. *Surf. Sci.* **2001**, *480*, 153–162.
[15] R. Zdyb, A. Pavlovska, M. Jałochowski, E. Bauer. *Surf. Sci.* **2006**, *600*, 1586.
[16] L. Le Guyader, K. Armin, A. Fraile Rodríguez, S. El Moussaoui, A. Balan, M. Buzzi, J. Raabe, F. Nolting. Studying nanomagnets and magnetic heterostructures with X-ray PEEM at the Swiss Light Source. *J. Electron. Spectrosc. Relat. Phenom.* **2012**, *185*, 371–380.
[17] V. Grolier, D. Renard, B. Bartenlian, P. Beauvillain, C. Chappert, C. Dupas, J. Ferré, M. Galtier, E. Kolb, M. Mulloy, J. P. Renard, P. Veillet. Unambiguous evidence of oscillatory magnetic coupling between Co layers in ultrahigh vacuum grown Co/Au(111)/Co trilayers. *Phys. Rev. Lett.* **1993**, *71*, 3023.
[18] J. Kurde, J. Miguel, D. Bayer, J. Sánchez-Barriga, F. Kronast, M. Aeschlimann, H. A. Dürr, W. Kuch. Magnetostatic coupling of 90 domain walls in $Fe_{19}Ni_{81}$/Cu/Co trilayers. *New J. Phys.* **2011**, *13*, 033015.
[19] E. S. Reich. *Nature* **2013**, *501*, 148–149.